 doi:10.20944/preprints202112.0428.v2

Communication

Application of Advanced Land Observing Satellite 3 (ALOS-3) Data to Land Cover and Vegetation Mapping

Ram C. Sharma*, Hidetake Hirayama and Keitarou Hara

Department of Informatics, Tokyo University of Information Sciences, 4-1 Onaridai, Wakaba-ku, Chiba 265-8501, Japan; sharma@rsch.tuis.ac.jp, hh207501@rsch.tuis.ac.jp, hara@rsch.tuis.ac.jp
*Correspondence: sharma@rsch.tuis.ac.jp; Tel.: +81-43-236-4603.

Abstract: Japan Aerospace Exploration Agency (JAXA) is going to launch Advanced Land Observing Satellite 3 (ALOS-3) after 2022. ALOS-3 satellite is capable of observing global land areas with wide swath (4000 km along-track direction and 70 km cross-track direction) at high spatial resolution (panchromatic: 0.8m, multispectral: 3.2m). Maintenance and updating of land cover and vegetation information at national level is one of the major goals of the ALOS-3 mission. This paper presents the potential of simulated ALOS-3 images for the classification and mapping of land cover and vegetation types at Genus-Physiognomy-Ecosystem (GPE) level. We acquired and simulated WorldView-3 images according to the configuration of the ALOS-3 satellite sensor and the simulated ALOS-3 images were utilized for the classification and mapping of land cover and vegetation types in three sites (Hakkoda, Zao, and Shiranuka) in northern Japan. This research dealt with 17 land cover and vegetation types in Hakkoda site, 25 land cover and vegetation types in Zao site, and 12 land cover and vegetation types in Shiranuka site. Ground truth data were newly collected in three sites, and we employed eXtreme Gradient Boosting (XGBoost) classifier with the implementation of 10-fold cross-validation method for assessing the potential of ALOS-3S images. The classification accuracies obtained in Hakkoda, Zao, and Shiranuka sites in terms of f1-score were 0.810, 0.729, and 0.805 respectively. The fine scale (3.2m) land cover and vegetation maps produced in the study sites showed clear and detailed view of the distribution of plant communities. Regardless of the limited number of the temporal images, ALOS-3S images showed high potential (at least 0.729 F1-score) for the land cover and vegetation classification in all three sites. The availability of more cloud free temporal scenes is expected for improved classification and mapping in the future.

Keywords: ALOS-3, Land Cover, Vegetation, Machine learning, Classification, Mapping, Genus-Physiognomy-Ecosystem level

1. Introduction

Japan Aerospace Exploration Agency (JAXA) is going to launch Advanced Land Observing Satellite 3 (ALOS-3) after 2022. The ALOS-3 satellite mission aims to deliver operational support services in the areas of disaster monitoring, updating geospatial information, and environmental monitoring. ALOS-3 is an advanced optical satellite, which carries an optical sensor complement to succeed PRISM (Panchromatic Remote-sensing Instrument for Stereo Mapping) and AVNIR-2 (Advanced Visible and Near-Infrared Radiometer-2) onboard the ALOS-1 satellite. It is capable of observing global land areas with wide swath (4000 km along-track direction and 70 km cross-track direction) at high spatial resolution (Panchromatic: 0.8m, Multispectral: 3.2m). Such a wide-swath width and revisit period of 35 days is a unique characteristic of the ALOS-3 satellite sensor.

Land cover is the prominent biophysical materials at the surface of the earth such as water, vegetation, barren, and built-up areas. The monitoring of land cover and vegetation

Preprints (www.preprints.org) | NOT PEER-REVIEWED | Posted: 13 May 2022 doi:10.20944/preprints202112.0428.v2

types is necessary for improved understanding of the carbon cycle and climate dynamics (Bounoua et al., 2002; Jung et al., 2006; Duveiller et al., 2018). It is also a key information necessary for habitat and biodiversity conservation and management practices (Xie et al., 2008; Grekousis et al., 2015).

According to the previous study (Sharma, 2021), vegetation types can be categorized into the following three hierarchical levels. (i) Land Cover level (Loveland et al., 2000): It is the classification at broad groups, for example, Water, Forest, Cultivated land, Built-up, and Barren land; (ii) Physiognomic level (Küchler, 1949): It includes division of the vegetation types into physiognomic level, for example, Evergreen Conifer Forest (ECF), Evergreen Broadleaf Forest (EBF), Deciduous Conifer Forest (DCF), Deciduous Broadleaf Forest (DBF), Grassland, and Shrubland; and (iii) Genus-Physiognomy-Ecosystem (GPE) level (Sharma, 2021). Here, vegetation physiognomic types are divided into plant community level with the inference of Genus/Physiognomy/Ecosystem. For example, Quercus EBF, Quercus DBF, Quercus Shrub, Fagus DBF, etc.

The major objective of this research is to present the potential of ALOS-3S images for land cover and vegetation classification and mapping at Genus-Physiognomy-Ecosystem (GPE) level, by employing the machine learning and cross-validation technique; and to discuss the superiority of high-resolution land cover and vegetation maps produced from the ALOS-3S images.

2. Materials and Methods

2.1. Study area

This research was conducted in three sites, Hakkoda, Zao, and Shiranuka located in Aomori, Miyagi, and Hokkaido prefectures respectively. These sites represent mountainous cool temperate forest ecosystems in Northern Japan. The location map of the study sites is shown in Figure 1.

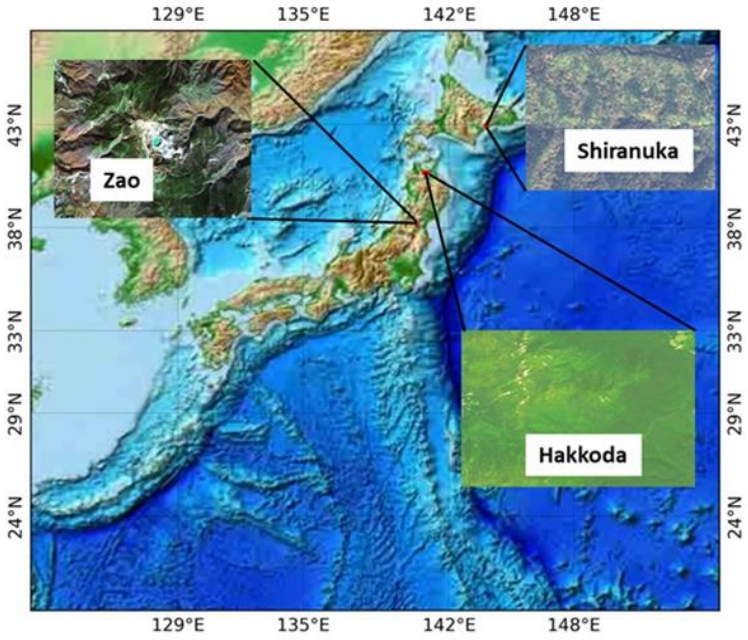

Figure 1. *Location map of the study sites. ALOS-3 Simulated (ALOS-3S) true-color images are shown for each site.*

Preprints (www.preprints.org) | NOT PEER-REVIEWED | Posted: 13 May 2022 doi:10.20944/preprints202112.0428.v2

2.2. Collection of ground truth data

The ground truth data were prepared by field survey, accompanied with existing vegetation survey map (1:25,000 scale) and visual interpretation of the time-lapse images available in Google Earth. For each land cover and vegetation type, 1200-2400 sample points (longitudes and latitudes), representing a homogenous area of at least 90×90m, were prepared for all sites concerned.

The list of land cover and vegetation types dealt in the research for Hakkoda, Zao, and Shiranuka sites are shown in Tables 1-3 respectively. This research adopts the Genus-Physiognomy-Ecosystem (GPE) system for the organization of vegetation types (Sharma, 2021).

***Table 1**. List of land cover and vegetation types of Hakkoda site.*

Land cover and vegetation classes	
1. Abies ECF	10. Pinus ECF
2. Alnus DBF	11. Open-space Herb
3. Barren	12. Deciduous Shrub
4. Betula DBF	13. Pinus Shrub
5. Cryptomeria ECF	14. Quercus DBF
6. Fagus DBF	15. Quercus Shrub
7. Larix DCF	16. Sasa Shrub
8. Miscanthus Herb	17. Wetland Herb
9. Juglans DBF	

DBF: Deciduous Broadleaf Forest; DCF: Deciduous Conifer Forest;
ECF: Evergreen Conifer Forest; EBF: Evergreen Broadleaf Forest

***Table 2**. List of land cover and vegetation types of Zao site.*

Land cover and vegetation classes	
1. Abies ECF	14. Open-space Herb
2. Acer DBF	15. Deciduous Shrub
3. Alnus DBF	16. Pinus ECF
4. Alpine Herb	17. Pinus Shrub
5. Alpine Shrub	18. Pterocarya DBF
6. Barren	19. Quercus DBF
7. Betula DBF	20. Quercus Shrub
8. Built-up	21. Salix Shrub
9. Cryptomeria ECF	22. Sasa Shrub
10. Fagus DBF	23. Tsuga ECF
11. Hydrangea Shrub	24. Water
12. Larix DCF	25. Wetland Herb
13. Miscanthus Herb	

DBF: Deciduous Broadleaf Forest; DCF: Deciduous Conifer Forest;
ECF: Evergreen Conifer Forest; EBF: Evergreen Broadleaf Forest

Preprints (www.preprints.org) | NOT PEER-REVIEWED | Posted: 13 May 2022 doi:10.20944/preprints202112.0428.v2

Table 3. *List of land cover and vegetation types of Shiranuka site.*

Land cover and vegetation classes	
1. Abies ECF	7. Salix DBF
2. Barren	8. Quercus DBF
3. Built-up	9. Sasa Shrub
4. Deciduous Shrub	10. Ulmus DBF
5. Larix DCF	11. Water
6. Pasture	12. Wetland Herb

DBF: Deciduous Broadleaf Forest; DCF: Deciduous Conifer Forest;
ECF: Evergreen Conifer Forest; EBF: Evergreen Broadleaf Forest

2.3. Generation of ALOS-3 images

We acquired eight image scenes for all three sites taken by WorldView-3 satellite which were more or less cloud free. The acquisition dates of satellite images and number of scenes utilized for each site have been shown in Table 4.

Table 4. *Satellite image acquisition dates and number of scenes utilized for each site.*

Hakkoda	Zao	Shiranuka
1. 2015-07-07	1. 2017-09-08	1. 2020-10-16
2. 2016-06-10	2. 2017-10-26	2. 2021-05-07
3. 2019-09-20		3. 2021-06-01

The WorldView-3 is a high-resolution commercial imaging satellite which acquires 11-bit data in 9 spectral bands (panchromatic, coastal, blue, green, yellow, red, red edge, near infrared 1, and near infrared 2), and additional 14-bits data in eight shortwave infrared bands. The nominal ground sample distance of the acquired images were 0.5 m for panchromatic and 2.0 m for multispectral images. We performed ortho-rectification of the WorldView-3 images with 30m digital elevation model data to remove geometric distortions.

The band wise Radiometric Calibration Factor (RCF) and Effective Band Width (EBW) data were read from the metadata of the given WorldView-3 products and Top-Of-Atmosphere (TOA) radiance was calculated from the pixel-wise Digital Number (DN) values using Equation (1).

$$\text{Radiance } (TOA) = \text{DN} \times \frac{\text{RCF}}{\text{EBW}} \qquad \text{Equation (1)}$$

Then, the TOA reflectance was calculated with Earth-Sun Distance (ESD), band-averaged Solar Spectral Irradiance (Irr), and Solar Zenith Angle (SZA) using Equation (2).

$$\text{Reflectance } (TOA) = \frac{\text{Radiance} \times ESD^2 \times 3.1416}{Irr \times Cos\ (SZA)} \qquad \text{Equation (2)}$$

Table 5 shows the band wise comparison between WorldView-3 (besides shortwave infrared bands) and ALOS-3 satellites. The observation bands between the WorldView-3 and ALOS-3 satellites are almost identical except for two bands (yellow and near infrared 2) which are not installed in ALOS-3.

Preprints (www.preprints.org) | NOT PEER-REVIEWED | Posted: 13 May 2022 doi:10.20944/preprints202112.0428.v2

Table 5. *Comparison of observation bands between WorldView-3 (besides shortwave infrared bands) and ALOS-3 satellites*

Bands	WorldView-3 (μm)	ALOS-3 (μm)
Coastal	0.40 ~ 0.45	0.40 ~ 0.45
Blue	0.45 ~ 0.51	0.45 ~ 0.50
Green	0.51 ~ 0.58	0.52 ~ 0.60
Yellow	0.58 ~ 0.62	not installed
Red	0.63 ~ 0.69	0.61 ~ 0.69
Red edge	0.70 ~ 0.74	0.69 ~ 0.74
Near infrared 1	0.77 ~ 0.89	0.76 ~ 0.89
Near infrared 2	0.86 ~ 1.04	not installed
Panchromatic	0.45 ~ 0.80	0.52 ~ 0.76

For this research, we extracted seven bands (coastal, blue, green, red, red edge, near infrared, and panchromatic) from the WorldView-3 satellite data which will be available from the ALOS-3 satellite. The WorldView-3 imagery were resampled into the size of the ALOS-3 satellite imagery (0.80 m for the panchromatic and 3.2 m for the multi-spectral bands) using nearest neighbor method. The resulting simulated (S) image is hereafter referred to as ALOS-3S image. In addition, we calculated nine spectral vegetation indices (as shown in Table 6) for each ALOS-3S scene.

Table 6. *Spectral vegetation indices utilized in the research.*

Indices	Formula	References
Normalized Difference Vegetation Index (NDVI)	$\frac{N-R}{N+R}$	Rouse et al., 1974
Green Red Vegetation Index (GRVI)	$\frac{G-R}{G+R}$	Falkowski et al., 2005
Soil-Adjusted Vegetation Index (SAVI)	$\frac{1.5\ \times (N-R)}{N+R+0.5}$	Huete., 1988
Modified Soil Adjusted Vegetation Index (MSAVI)	$\frac{2N+1-\sqrt{(2N+1)^2-8(N-R)}}{2}$	Qi et al., 1994
Atmospherically Resistant Vegetation Index (ARVI)	$\frac{N-R-(R-B)}{N+R-(R-B)}$	Kaufman and Tanre, 1992
Modified Chlorophyll Absorption Ratio Index (MCARI)	$\{(RE-R)-0.2(RE-G)\}(RE/R)$	Daughtry et al., 2000

Preprints (www.preprints.org) | NOT PEER-REVIEWED | Posted: 13 May 2022 doi:10.20944/preprints202112.0428.v2

Non-Homogeneous Feature Difference (NHFD)	$\frac{RE - C}{RE + C}$	Wolf, 2012
Structure-Insensitive Pigment Index (SIPI)	$\frac{N - B}{N - R}$	Penuelas et al., 1995
Enhanced Vegetation Index (EVI)	$2.5\frac{N - R}{(N + 6R - 7.5B) + 1}$	Huete et al., 2002

The multi-temopral features comprising of spectral and vegetation indices were prepared for machine learning. It comprised of 48 features (3 observations × 16 bands) for the Hakkoda and Shiranuka sites and 32 features (2 observations × 16 bands) for the Zao site.

2.4. Machine learning and mapping

The pixel values, corresponding to the ground truth (geolocation points) were extracted from the ALOS-3S feature images. eXtreme Gradient Boosting (XGBoost) classifier was employed for the supervised classiifaction of the satellite data. We applied train-test split method (75% traing data, 25% test data) for assessing the potential of ALOS-3S data for the classification of land cover and vegetation types. Classification accuracy metrics, such as overall accuracy, kappa coefficient, F1-score, recall, and precision were calculated for quantatative assessment of the model performance. The model trained on 75% data was used for the prediction (mapping) on new datasets.

3. Results and Discussion

3.1. Confusion matrices

The confusion matrix figures calculated for the Hakkoda, Zao, and Shiranuka sites have been shown in Figures 2-4 respectively.

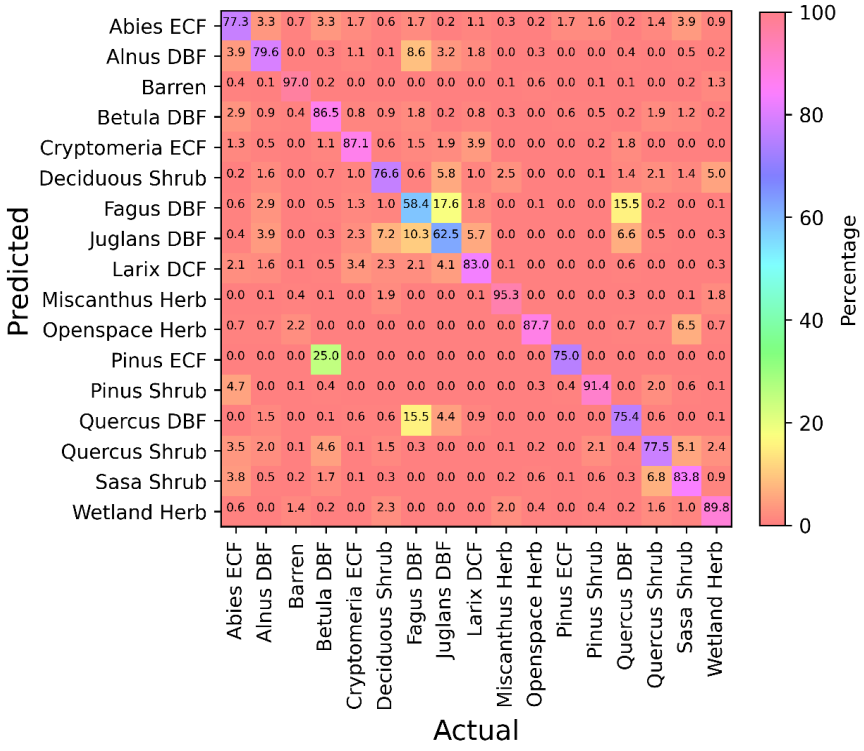

Figure 2. The confusion matrix computed for the Hakkoda site.

Preprints (www.preprints.org) | NOT PEER-REVIEWED | Posted: 13 May 2022 doi:10.20944/preprints202112.0428.v2

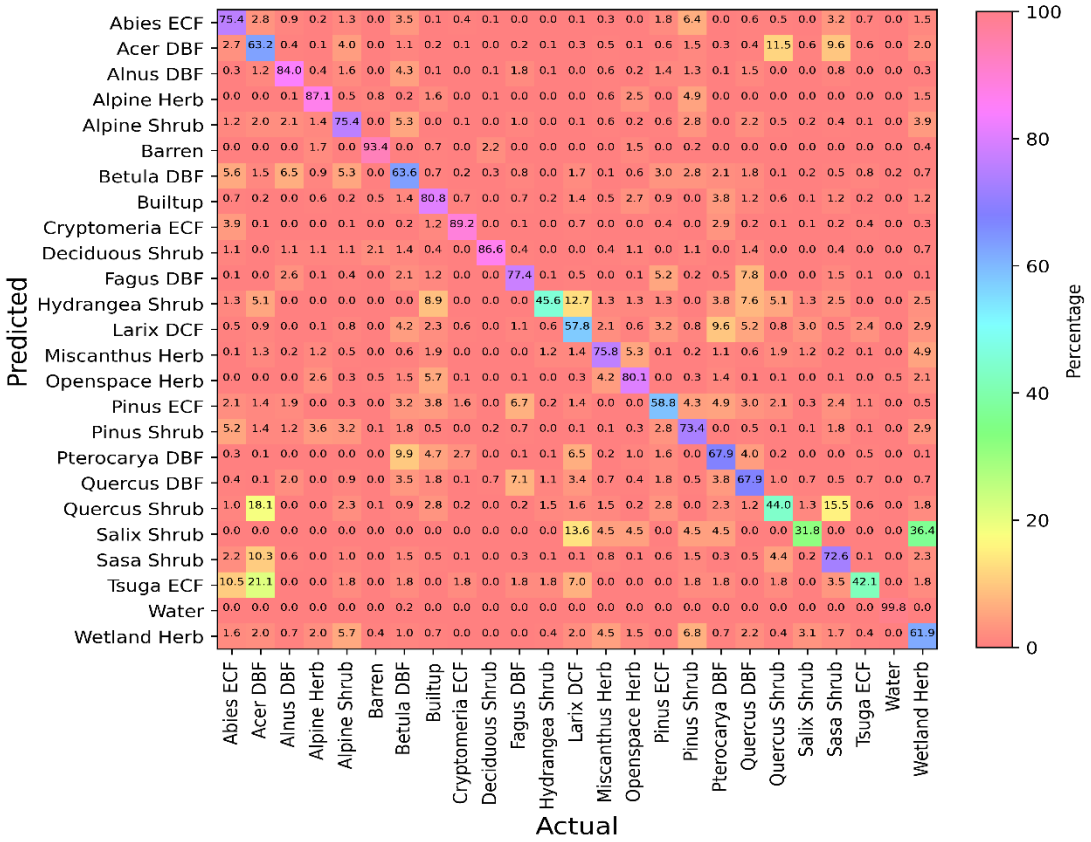

Figure 3. The confusion matrix computed for the Zao site.

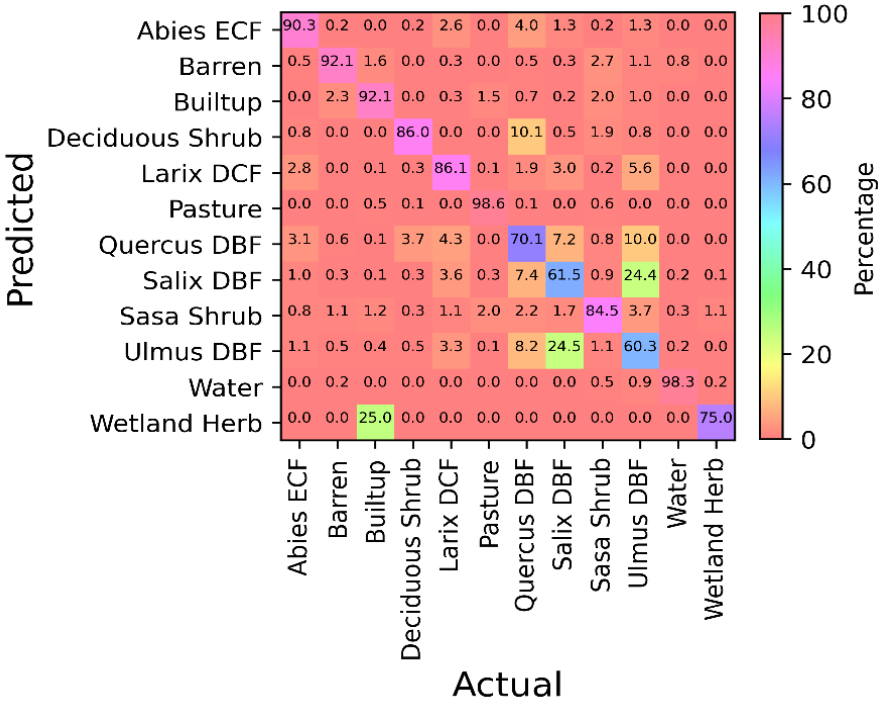

Figure 4. The confusion matrix computed for the Shiranuka site.

3.2. Class wise accuracies

Tables 7-9 show the class-wise accuracy for Hakkoda, Zao, and Shiranuka sites respectively.

Preprints (www.preprints.org) | NOT PEER-REVIEWED | Posted: 13 May 2022 doi:10.20944/preprints202112.0428.v2

Table 7. *Class wise accuracy obtained for the Hakkoda site.*

Class	Accuracy	Kappa	Precision	Recall	F1-score
Abies ECF	0.964	0.765	0.773	0.798	0.785
Alnus DBF	0.980	0.707	0.796	0.653	0.717
Barren	0.996	0.957	0.970	0.949	0.959
Betula DBF	0.978	0.855	0.865	0.869	0.867
Cryptomeria ECF	0.988	0.833	0.871	0.811	0.840
Deciduous Shrub	0.979	0.743	0.766	0.742	0.754
Fagus DBF	0.934	0.604	0.584	0.709	0.641
Juglans DBF	0.959	0.49	0.625	0.432	0.511
Larix DCF	0.982	0.823	0.83	0.836	0.833
Miscanthus Herb	0.994	0.941	0.953	0.936	0.945
Open-space Herb	0.997	0.762	0.877	0.676	0.763
Pinus ECF	0.998	0.141	0.750	0.078	0.141
Pinus Shrub	0.989	0.919	0.914	0.936	0.925
Quercus DBF	0.959	0.728	0.754	0.748	0.751
Quercus Shrub	0.967	0.789	0.775	0.842	0.808
Sasa Shrub	0.975	0.836	0.838	0.862	0.85
Wetland Herb	0.983	0.889	0.898	0.899	0.899
Overall	0.810	0.795	0.810	0.810	0.810

Table 8. *Class wise accuracy obtained for the Zao site.*

Class	Accuracy	Kappa	Precision	Recall	F1-score
Abies ECF	0.971	0.746	0.754	0.769	0.761
Acer DBF	0.958	0.650	0.632	0.719	0.673
Alnus DBF	0.983	0.803	0.840	0.786	0.812
Alpine Herb	0.986	0.879	0.871	0.902	0.886
Alpine Shrub	0.977	0.704	0.754	0.681	0.716
Barren	0.998	0.918	0.934	0.904	0.919
Betula DBF	0.955	0.592	0.636	0.598	0.616
Built-up	0.975	0.781	0.808	0.780	0.794
Cryptomeria ECF	0.992	0.900	0.892	0.917	0.905
Deciduous Shrub	0.998	0.847	0.866	0.831	0.848
Fagus DBF	0.976	0.796	0.774	0.846	0.809
Hydrangea Shrub	0.996	0.309	0.456	0.235	0.310
Larix DCF	0.953	0.653	0.578	0.818	0.677
Miscanthus Herb	0.978	0.803	0.758	0.879	0.814
Open-space Herb	0.987	0.692	0.801	0.619	0.698
Pinus ECF	0.978	0.438	0.588	0.363	0.449
Pinus Shrub	0.968	0.724	0.734	0.749	0.741
Pterocarya DBF	0.963	0.659	0.679	0.678	0.679
Quercus DBF	0.962	0.668	0.679	0.698	0.688

Preprints (www.preprints.org) | NOT PEER-REVIEWED | Posted: 13 May 2022 doi:10.20944/preprints202112.0428.v2

Quercus Shrub	0.972	0.429	0.440	0.447	0.444
Salix Shrub	0.994	0.054	0.318	0.03	0.054
Sasa Shrub	0.97	0.668	0.726	0.646	0.684
Tsuga ECF	0.994	0.162	0.421	0.102	0.164
Water	0.999	0.994	0.998	0.991	0.994
Wetland Herb	0.977	0.465	0.619	0.387	0.476
Overall	0.729	0.714	0.729	0.729	0.729

Table 9. *Class wise accuracy obtained for the Shiranuka site.*

Class	Accuracy	Kappa	Precision	Recall	F1-score
Abies ECF	0.974	0.893	0.903	0.914	0.908
Barren	0.995	0.871	0.921	0.832	0.874
Builtup	0.994	0.912	0.921	0.910	0.916
Deciduous Shrub	0.989	0.767	0.860	0.702	0.773
Larix DCF	0.961	0.839	0.861	0.863	0.862
Pasture	0.996	0.982	0.986	0.983	0.985
Quercus DBF	0.922	0.693	0.701	0.780	0.739
Salix DBF	0.911	0.490	0.615	0.479	0.538
Sasa Shrub	0.982	0.860	0.845	0.896	0.869
Ulmus DBF	0.890	0.561	0.603	0.650	0.625
Water	0.998	0.976	0.983	0.971	0.977
Wetland Herb	0.999	0.261	0.750	0.158	0.261
Overall	0.805	0.779	0.805	0.805	0.805

3.3. Performance summary

The performance of ALOS-3S images on the classification of land cover and vegetation types in all three study sites (Hakkoda, Zao, and Shiranuka) has been summarized in Table 10.

Table 10. *Summary of the performance of ALOS-3S images.*

Site	Overall accuracy	Kappa coefficient	F1-score	Recall	Precision
Hakkoda	0.810	0.795	0.810	0.810	0.810
Zao	0.729	0.714	0.729	0.729	0.729
Shiranuka	0.805	0.779	0.805	0.805	0.805

Though most of the classes were discriminated satisfactorily, weak classification of some classes, for instance Juglans DBF and Pinus ECF in site Hakkoda (Table 7), Salix Shrub and Tsuga ECF in site Zao (Table 8), and Salix DBF and Wetland Herb in site Shiranuka (Table 9) were detected.

3.4. Production of LCV maps

The land cover and vegetation maps produced in the research have been shown in Figures 5-7 for Hakkoda, Zao, and Shiranuka sites respectively. The fine scale (3.2m) land cover and vegetation maps produced in our research has clearly shown the detailed view and distribution of plant communities.

Preprints (www.preprints.org) | NOT PEER-REVIEWED | Posted: 13 May 2022 doi:10.20944/preprints202112.0428.v2

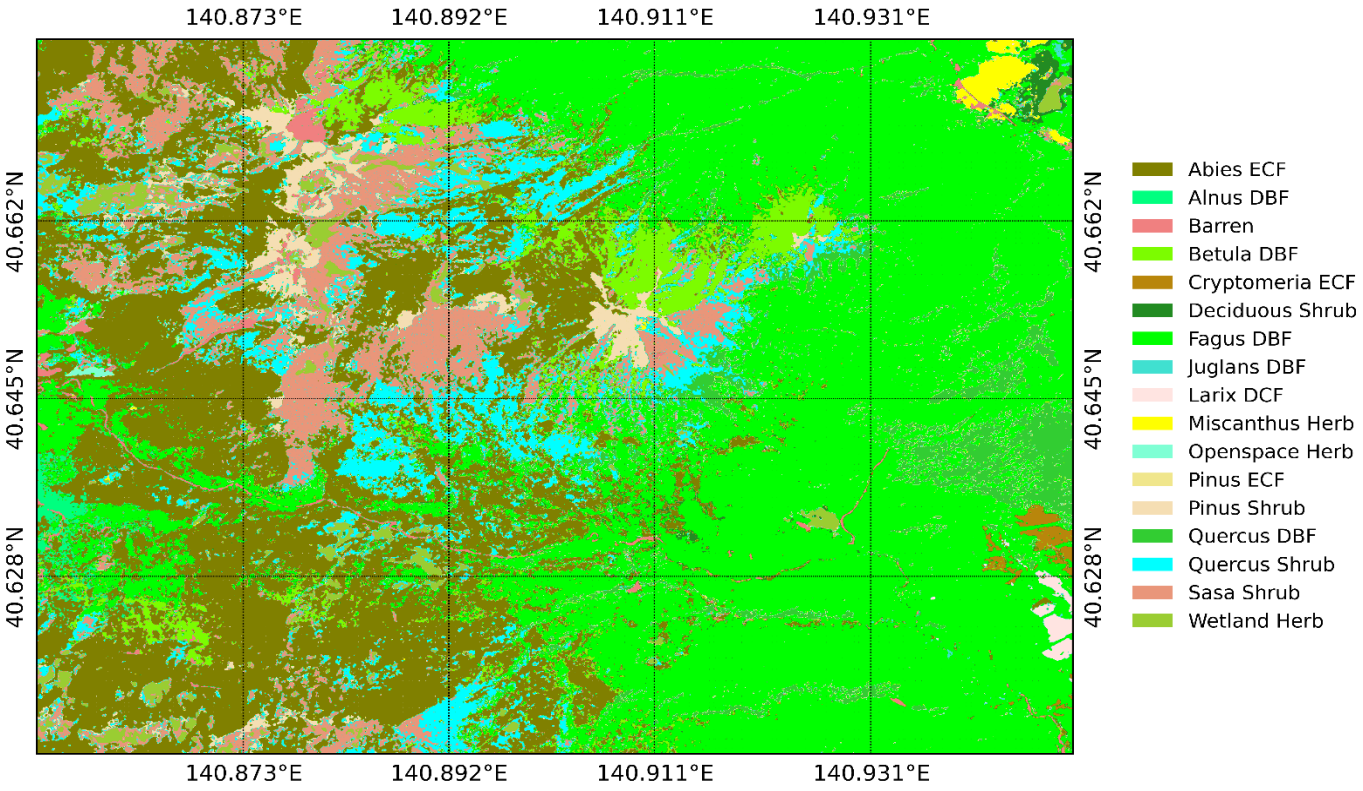

Figure 5. 17-class land cover and vegetation map of Hakkoda site using ALOS-3S images.

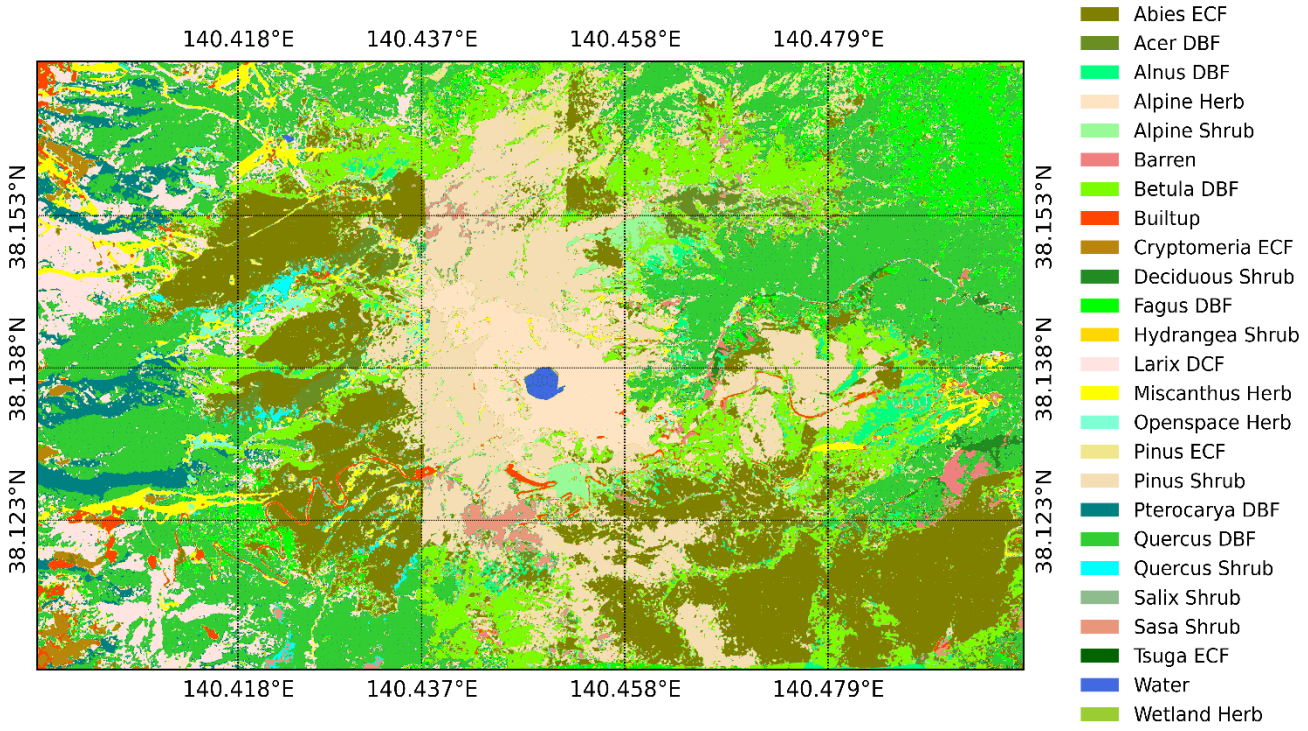

Figure 6. 25-class land cover and vegetation map of Zao site using ALOS-3S images.

Preprints (www.preprints.org) | NOT PEER-REVIEWED | Posted: 13 May 2022 doi:10.20944/preprints202112.0428.v2

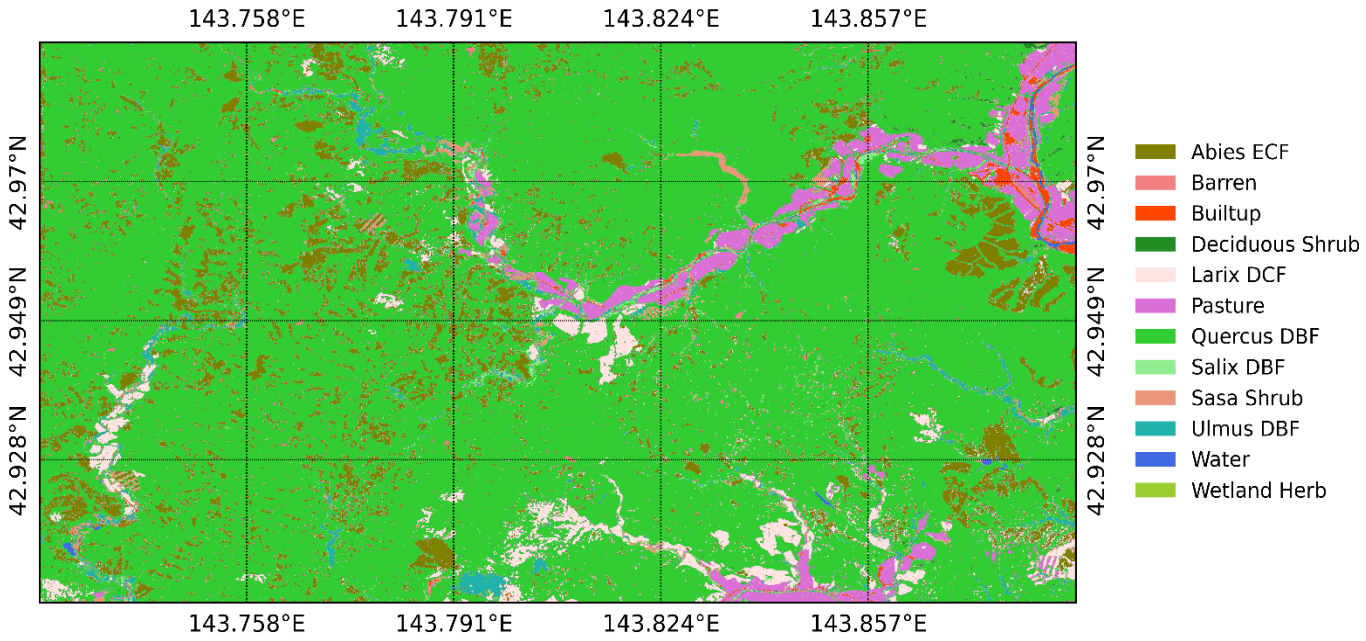

Figure 7. 12-class land cover and vegetation map of Shiranuka site using ALOS-3S images.

In this research, we conducted classification and mapping of land cover and vegetation types by employing eXtreme Gradient Boosting (XGBoost) classifier on the ALOS-3S images. The availability of more cloud-free temporal scenes is expected to be available after the launch of ALOS-3 satellite to grasp seasonal information for improving the classification further. Moreover, as the ALOS-3 satellite is also capable of acquiring stereo-pair image, high-resolution digital surface models are expected for better understanding the distribution of vegetation types.

ALOS-3 satellite has the capacity of viewing a large region of interest with similar weather and atmospheric conditions at a time due to wide-swath (4000 km along-track direction and 70 km cross-track direction) of the satellite with the possible benefits for land cover and vegetation mapping in contrast to images acquired from narrow-swath satellites with different weather conditions. Moreover, the high-spatial resolution (0.8m panchromatic and 3.2m multi-spectral) images offerred by the ALOS-3 satellite can segment the plant communities into individual crown level which is important for detection and mapping of small patches of plant communities such as alpine herbs which are difficult to detect from coarse resolution images such as Sentinel-2. However, spatio-temporal fusion of high-temporal (5 days) but coarse-spatial resolution (10m) Sentinel-2 images with high-spatial resolution (3.2m) but low-temporal resolution (35days) ALOS-3 images can offer land cover and vegetation mapping at a fine scale.

4. Conclusion

Seamless observation of global land surface with 35-days revisit period by ALOS-3 satellite will be one of the highest capacity available for the high-resolution (panchromatic 0.8m, multi-spectral 3.2m) satellites. In this research, we assessed the potential of ALOS-3S images with limited temporal scenes for the classification and mapping of land cover

and vegetation types in three cool-temperate sites in northeastern Japan. Achieving at least 72% classification accuracy in terms of F1-score with limited temporal scenes is promising. Availability of more temporal scenes from the ALOS-3 satellite is expected for improved land cover and vegetation mapping at a country scale in the future.

Author Contributions: R. C. Sharma conceived the research, performed the research, and wrote the manuscript. H. Hirayama supported data processing. K. Hara supervised the research and provided valuable discussions. All authors have read and agreed to the published version of the manuscript.

Funding: This research was conducted under the framework of JAXA commissioned research (Application of ALOS-3 satellite data to vegetation mapping in 2019-2021). The preparation of ground truth data was supported by the commissioned research of the Ministry of the Environment, Center for Biodiversity and Asia Air Survey Co., Ltd. This research was partially supported by JSPS Grant-in-Aid for Scientific Research (JP19H04320).

Acknowledgments: Copyright of the WorldView-3 data is inherited to Maxar (formally DigitalGlobe).

Conflicts of Interest: The authors declare no conflict of interest.

References

1. Bounoua, L.; DeFries, R.; Collatz, G.J.; Sellers, P.; Khan, H. Effects of Land Cover Conversion on Surface Climate. *Climatic Change* 2002, *52*, 29–64, doi:10.1023/A:1013051420309.
2. Daughtry, C. Estimating Corn Leaf Chlorophyll Concentration from Leaf and Canopy Reflectance. *Remote Sensing of Environment* 2000, *74*, 229–239, doi:10.1016/S0034-4257(00)00113-9.
3. Duveiller, G.; Caporaso, L.; Abad-Viñas, R.; Perugini, L.; Grassi, G.; Arneth, A.; Cescatti, A. Local Biophysical Effects of Land Use and Land Cover Change: Towards an Assessment Tool for Policy Makers. *Land Use Policy* 2020, *91*, 104382, doi:10.1016/j.landusepol.2019.104382.
4. Falkowski, M.J.; Gessler, P.E.; Morgan, P.; Hudak, A.T.; Smith, A.M.S. Characterizing and Mapping Forest Fire Fuels Using ASTER Imagery and Gradient Modeling. *Forest Ecology and Management* 2005, *217*, 129–146, doi:10.1016/j.foreco.2005.06.013.
5. Grekousis, G.; Mountrakis, G.; Kavouras, M. An Overview of 21 Global and 43 Regional Land-Cover Mapping Products. *International Journal of Remote Sensing* 2015, *36*, 5309–5335, doi:10.1080/01431161.2015.1093195.
6. Huete, A.; Didan, K.; Miura, T.; Rodriguez, E.P.; Gao, X.; Ferreira, L.G. Overview of the Radiometric and Biophysical Performance of the MODIS Vegetation Indices. *Remote Sensing of Environment* 2002, *83*, 195–213, doi:10.1016/S0034-4257(02)00096-2.
7. Huete, A.R. A Soil-Adjusted Vegetation Index (SAVI). *Remote Sensing of Environment* 1988, *25*, 295–309, doi:10.1016/0034-4257(88)90106-X.
8. Jung, M.; Henkel, K.; Herold, M.; Churkina, G. Exploiting Synergies of Global Land Cover Products for Carbon Cycle Modeling. *Remote Sensing of Environment* 2006, *101*, 534–553, doi:10.1016/j.rse.2006.01.020.
9. Kaufman, Y.J.; Tanre, D. Atmospherically Resistant Vegetation Index (ARVI) for EOS-MODIS. *IEEE Trans. Geosci. Remote Sensing* 1992, *30*, 261–270, doi:10.1109/36.134076.
10. Küchler, A.W. A Physiognomic Classification of Vegetation. *Annals of the Association of American Geographers* 1949, *39*, 201–210, doi:10.1080/00045604909352005
11. Loveland, T.R.; Reed, B.C.; Brown, J.F.; Ohlen, D.O.; Zhu, Z.; Yang, L.; Merchant, J.W. Development of a Global Land Cover Characteristics Database and IGBP DISCover from 1 Km AVHRR Data. *International Journal of Remote Sensing* 2000, *21*, 1303–1330, doi:10.1080/014311600210191.
12. Penuelas, J.; Frederic, B.; Filella, I. Semi-Empirical Indices to Assess Carotenoids/Chlorophyll-a Ratio from Leaf Spectral Reflectance. *Photosynthetica* 1995, *31*, 221–230.

 doi:10.20944/preprints202112.0428.v2

13. Qi, J.; Chehbouni, A.; Huete, A.R.; Kerr, Y.H.; Sorooshian, S. A Modified Soil Adjusted Vegetation Index. *Remote Sensing of Environment* 1994, *48*, 119–126, doi:10.1016/0034-4257(94)90134-1.
14. Rouse, J.W.; Haas, R.H.; Schell, J.A.; Deering, D.W. Monitoring Vegetation Systems in the Great Plains with ERTS. *NASA special publication* 1974, *351*, 309.
15. Sharma, R.C. Genus-Physiognomy-Ecosystem (GPE) System for Satellite-Based Classification of Plant Communities. *Ecologies* 2021, *2*, 203–213, doi:10.3390/ecologies2020012.
16. Wolf, A.F. Using WorldView-2 Vis-NIR Multispectral Imagery to Support Land Mapping and Feature Extraction Using Normalized Difference Index Ratios.; Shen, S.S., Lewis, P.E., Eds.; Baltimore, Maryland, May 1 2012; pp. 83900N-83900N – 8.
17. Xie, Y.; Sha, Z.; Yu, M. Remote Sensing Imagery in Vegetation Mapping: A Review. *Journal of Plant Ecology* 2008, *1*, 9–23, doi:10.1093/jpe/rtm005.